Appl Magn Reson (2010) 38:349–360
DOI 10.1007/s00723-010-0124-1

Applied
Magnetic Resonance

Assessment of Blood Hemodynamics by USPIO-Induced R_1 Changes in MRI of Murine Colon Carcinoma

Giulio Gambarota · H. W. M. van Laarhoven · M. Philippens · W. J. M. Peeters · P. Rijken · A. van der Kogel · C. J. A. Punt · A. Heerschap

Received: 2 January 2010 / Revised: 1 February 2010 / Published online: 28 March 2010

Abstract The objective of this study is to assess whether ultrasmall superparamagnetic iron oxide (USPIO)-induced changes of the water proton longitudinal relaxation rate (R_1) provide a means to assess blood hemodynamics of tumors. Two types of murine colon tumors (C26a and C38) were investigated prior to and following administration of USPIO blood-pool contrast agent with fast R_1 measurements. In a subpopulation of mice, R_1 was measured following administration of hydralazine, a well-known blood hemodynamic modifier. USPIO-induced R_1 increase in C38 tumors ($\Delta R_1 = 0.072 \pm 0.0081\ s^{-1}$) was significantly larger than in C26a tumors ($\Delta R_1 = 0.032 \pm 0.0018\ s^{-1}$, $N = 9$, t test, $P < 0.001$). This was in agreement with the immunohistochemical data that showed higher values of relative vascular area (RVA) in C38 tumors than in C26a tumors (RVA $= 0.059 \pm 0.015$ vs. 0.020 ± 0.011; $P < 0.05$). Following administration of hydralazine, a decrease

G. Gambarota · A. Heerschap
Department of Radiology, Radboud University Nijmegen Medical Centre, Nijmegen, The Netherlands

H. W. M. van Laarhoven · C. J. A. Punt
Department of Medical Oncology, Radboud University Nijmegen Medical Centre, Nijmegen, The Netherlands

M. Philippens · W. J. M. Peeters · P. Rijken · A. van der Kogel
Department of Radiation Oncology, Radboud University Nijmegen Medical Centre, Nijmegen, The Netherlands

Present Address:
G. Gambarota (✉)
GSK Clinical Imaging Centre, Imperial College, Hammersmith Hospital, Du Cane Road, London W12 0NN, UK
e-mail: gambarota@gmail.com

in R_1 value was observed. This was consistent with the vasoconstriction induced by the steal effect mechanism. In conclusion, R_1 changes induced by USPIO are sensitive to tumor vascular morphology and to blood hemodynamics. Thus, R_1 measurements following USPIO administration can give novel insight into the effects of blood hemodynamic modifiers, non-invasively and with a high temporal resolution.

1 Introduction

It is well established that tumor vasculature plays a key role in tumor growth [1]. Tumor vessels are not only morphologically, but also physiologically distinct from host vessels [2]. Knowledge about these aspects of tumor vasculature is critical to tumor therapy, both in novel anti-angiogenesis therapeutic treatments and in conventional cytotoxic therapy. Moreover, in recent studies, blood hemodynamic modifiers have been employed to enhance the effects of treatment [3]. However, the exact mechanism by which blood hemodynamic modifiers act is still not well understood [4] and their effects on tumor hemodynamics remain unclear [5]. It is crucial, therefore, to characterize the tumor vasculature and its response to blood hemodynamic modifiers in order to assess and improve the effectiveness of current therapeutic treatments.

Magnetic resonance imaging (MRI), in combination with contrast agent administration, has proven useful in the characterization of tumor vasculature. Several studies have shown that magnetic susceptibility effects, caused by blood-pool contrast agents that consist of ultrasmall superparamagnetic particles of iron oxide (USPIO), can be used to assess blood volume and vessel sizes within tumors. USPIOs have been mostly employed in combination with quantitative and/or qualitative T_2 and T_2* measurements [6–12]. In particular, the enhancement in the transverse relaxation rates R_2 (=1/T_2) and R_2* (=1/T_2*), after administration of USPIO, provides an index proportional to the blood volume of the microvasculature and macrovasculature, respectively. However, quantitative ΔR_2 and ΔR_2* measurements are characterized by relatively long acquisition times, due to the long repetition time TR needed to minimize T_1 effects.

Quantitative T_1 MRI, in combination with USPIO administration, represents an alternative approach to T_2/T_2* USPIO contrast-enhanced MRI, in particular, when fast assessment (i.e., on the order of seconds) of blood hemodynamics is needed. In this study, detailed measurements of changes in longitudinal relaxation rate R_1 (=1/T_1), following USPIO administration were performed within in vivo tumor tissue. R_1 was measured with the inversion–recovery snapshot fast low-angle shot (IR-FLASH) imaging sequence pre- and post-USPIO administration, in two different types of murine colon carcinoma (C26a, C38). The findings were compared with the vascularity of these tumor types as determined by immunohistochemistry. To assess whether USPIO-induced R_1 changes provide a means to assess blood hemodynamics with high temporal resolution, we administered hydralazine—a central vasodilator which induces vasoconstriction in subcutaneous tumors by the steal effect mechanism [13]—and monitored R_1 changes in time.

2 Materials and Methods

2.1 MRI

All procedures were approved by the Radboud University Nijmegen Medical Center Animal Care and Use Committee. C26a ($n = 9$) and C38 ($n = 9$) murine colon tumor tissue fragments were implanted subcutaneously in female Balb/C and C57/Bl6 mice, respectively, of 8–12 weeks of age. Experiments were performed when tumors reached the diameter of approximately 0.8 cm. Mice were anesthetized with isoflurane inhalation (1.5–2%); in each mouse, a catheter was inserted in the tail vein for the administration of the contrast agent and the tumor was positioned in the center of a 10-mm diameter surface radio-frequency (RF) coil used as a transmitter/receiver. During the measurements, the body temperature was monitored with a rectal fluoroptic probe (Luxtron 712, Luxtron Corporation, California, USA) and maintained at a constant temperature of 37 ± 1°C with a warm water pad.

MRI experiments were performed on a 7T/200 mm horizontal-bore MR spectrometer interfaced to a SMIS console and equipped with a gradient insert with a gradient strength of 150 mT/m and rise time of 150 μs. The image acquisition protocol started with three-gradient echo scout images followed by multislice gradient echo images for anatomical localization of the tumor. Imaging parameters were: repetition time (TR) = 400 ms, echo time (TE) = 10 ms, image matrix size of 128 × 128, field of view (FOV) of 5.8 cm × 5.8 cm, slice thickness (SLT) of 0.7 mm and 1 excitation per phase-encoding step. IR-FLASH imaging [14, 15] was then performed on a slice through the center of the tumor, prior to and following administration of an USPIO blood-pool contrast agent (Sinerem®, Guerbet, France; 150 μmol Fe/kg). Imaging parameters were: TR/TE = 5 ms/2.7 ms, image matrix size of 64 × 64, FOV of 3 cm × 3 cm, SLT of 1.6 mm. In this sequence, the longitudinal magnetization is first inverted by a hyperbolic secant adiabatic inversion pulse and then repeatedly sampled by a train of small flip-angle (5°) read-out Gaussian pulses to generate multiple images at different time points on the T_1 water proton recovery curve. Digitized RF spoiling pulses with phase angle increments of 117° [16], and a gradient spoiling were applied in order to spoil the transverse steady-state magnetization prior to each read-out pulse. The time interval between the inversion pulse and the first image was 52 ms. Ten dummy scans were applied prior to each image acquisition so that the total acquisition time per image was 370 ms. The lines in the **k**-space were acquired with a centric profile order to generate 16 images, which sampled the recovery of the longitudinal magnetization over ca. 5 s, at intervals of 370 ms.

To assess the precision of the R_1 measurement, in order to determine whether the changes in R_1 induced by the contrast agent are greater than the measurement error, four repeated R_1 measurements were performed prior to and following administration of USPIO on a group of mice ($n = 5$, C26a tumors and $n = 5$, C38 tumors). Further, in a group of mice with C38 tumors ($n = 3$), an intraperitoneal catheter was inserted for hydralazine injection. Hydralazine was dissolved in NaCl 0.9% to a concentration of 0.33 mg/ml and intraperitoneally injected at a dose of 2.5 mg/kg of mouse weight. The MRI protocol was as before with the only difference that after the post-USPIO R_1 measurement, hydralazine was injected, and the R_1 value was measured 5 min thereafter.

2.2 Data Analysis

The Levenberg–Marquardt non-linear least squares algorithm was used to analyze the R_1 relaxation data. R_1 maps were obtained from the entire set of 16 images. Voxel-by-voxel R_1 maps, pre- and post-USPIO, and after hydralazine, were generated from a three-parameter fit of the image intensities according to the equation: $S(\mathrm{TI}) = A + B\ \exp(-\mathrm{TI}/T_1{}^*)$ and the value of the corrected R_1 was calculated from the formula: $R_1 = (T_1{}^*(B/A - 1))^{-1}$ which is valid in the small flip-angle limit. Pixel-by-pixel T_1 maps were calculated using an algorithm described elsewhere [17]. First, for each pixel, the signal intensity of the 16 magnitude images was evaluated and the minimum value (S_{min}) was determined. Second, an inversion–recovery curve (i.e., with negative and positive values) was generated by inverting all the data on the left of the minimum value S_{min}. The fit was determined, as well as the coefficient of determination (R^2), which is a measure of the goodness of the fit. Third, the same procedure was repeated choosing one point on the left ($S_{\mathrm{min}-1}$) and one point on the right ($S_{\mathrm{min}+1}$) of S_{min}, so that two additional inversion–recovery curves were generated by inverting all the data on the left of ($S_{\mathrm{min}-1}$) and of ($S_{\mathrm{min}+1}$), respectively. The fit was determined, as well as R^2. Thus, in total, three inversion–recovery curves were generated. The inversion–recovery which displayed the best fit (i.e., highest R^2) was chosen for calculating the T_1 relaxation time. The fitting algorithm is further described in Ref. [17]. From the voxel-by-voxel R_1 maps, ΔR_1 maps ($\Delta R_1 = R_{1\mathrm{post}} - R_{1\mathrm{pre}}$, where $R_{1\mathrm{post}}$ and $R_{1\mathrm{pre}}$ are the R_1 post- and pre-USPIO, respectively) were calculated. For each tumor, the mean ΔR_1 was then calculated by drawing a region-of-interest (ROI)—which included the tumor core—on the ΔR_1 map and averaging the ΔR_1 values of all voxels within the ROI.

To assess the precision of the measured R_1 values, we performed four repeated measurements of R_1 prior to and following administration of USPIO. For each tumor, four R_1 maps pre-USPIO and four R_1 maps post-USPIO were generated as described in the previous paragraph. From each R_1 map, the mean R_1 was calculated by averaging the R_1 values of all voxels within an ROI which included the tumor core. The standard deviation (SD) over four repeated R_1 measurements, pre-USPIO and post-USPIO was calculated [18]. All data are expressed as mean $\pm$ SD. The Levenberg–Marquardt non-linear least squares algorithms were implemented in MatLab (Mathworks, Natick, MA, USA).

In order to compare the changes in the R_1 relaxation time (ΔR_1) in the C26a tumor with the ΔR_1 value in the C38 tumor line, the data were further analyzed with the software package Prism (GraphPad Software Inc., CA, USA). The statistical significance ($P < 0.001$) of differences between the ΔR_1 value in the C26a and C38 tumors was determined by means of a two-tailed Student's t test.

2.3 Theory

Since the USPIO remains intravascular, modeling of the effects of the USPIO on the R_1 relaxation rate requires the framework of a two-compartment exchange model, where the two compartments are the intra- and extravascular space. The relaxation behavior

of the two-compartment exchange model depends on the exchange rate τ^{-1}, defined as the sum of τ_i^{-1} and τ_e^{-1}, where τ_i and τ_e are the water proton lifetimes in the intra- and extravascular compartment, respectively, and on the absolute value of the difference between the water proton relaxation rates of the intra- and extravascular space (R_{1i} and R_{1e}, respectively). The precise value of τ^{-1} is not exactly known [19]; however, the reported values are ca. 1 Hz [20–23]. The two-compartment model is in slow exchange when the condition $\tau^{-1} \ll |R_{1i} - R_{1e}|$ is satisfied. Schwarzbauer et al. [24] showed that, following contrast agent administration, in the case of slow exchange the observed change in relaxation rate ΔR_1 is equal to PS/(λ − RBV), where PS is the permeability-surface area product for water across blood vessel walls, λ is the tissue-to-blood partition coefficient and RBV is the regional blood volume. For typical values of λ and RBV [24], RBV $\ll \lambda$ and therefore, after Taylor series expansion ($1/[1 - x] \sim [1 + x]$, for $|x| \ll 1$), $\Delta R_1 \sim (\mathrm{PS}/\lambda)(1 + \mathrm{RBV}/\lambda)$.

2.4 Immunohistochemistry

In two separate groups of mice ($n = 6$ for C38 and $n = 5$ for C26a) with tumors of approximately the same size as used for the MR experiments, tumor vascularity was determined by immunohistochemistry. After the animals were killed by cervical dislocation, their tumors were excised immediately and stored under liquid nitrogen. Frozen tumor sections of 5 μm thickness were cut for staining and further analysis of vasculature. After thawing, the sections were fixed in cold (4°C) acetone for 10 min. Between all consecutive steps of the staining procedure, sections were rinsed three times for 2 min in phosphate buffered saline. Sections were mounted in Fluorostab (Organon, Boxtel, The Netherlands). Endothelial structures were stained with 9F1, which is a rat monoclonal antibody to mouse endothelium (Department of Pathology, University Medical Centre Nijmegen, The Netherlands) [25]. Then sections were incubated for 30 min at 37°C with goat anti-rat-Alexa546 (Molecular Probes, Leiden, The Netherlands) and diluted 1:200 in polyclonal liquid diluent (Euro-DPC, Breda, The Netherlands). Quantitative data for tumor vascularity were acquired by a semiautomatic method based on a computerized digital image analysis system, as described previously [26, 27]. Whole tumor sections were scanned for 9F1 positive structures and a contour line was drawn to delineate the tumor area thereby excluding non-tumor tissue from the analyses. Consecutive hematoxylin and eosin-stained tumor sections were employed to distinguish parenchyma from non-tumor tissue. The resulting composite image was divided into smaller ROIs (230 × 230 μm). In each ROI the relative vascular area (RVA: 9F1 positive area divided by the viable tumor area) was calculated. From this, a new image map was created in which the voxels had values of the RVA values in the corresponding ROIs.

3 Results

The IR-FLASH provided a fast method for measuring the water proton R_1 relaxation rate in murine colon carcinoma. Figure 1 shows the sixteen IR-FLASH images of a

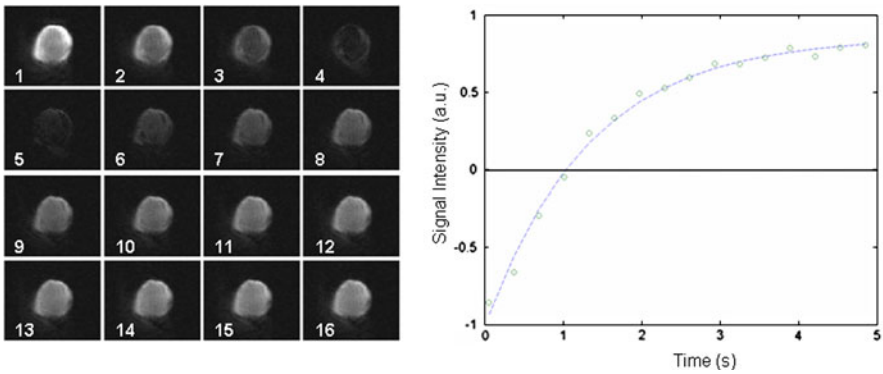

Fig. 1 IR-FLASH measurements of the R_1 relaxation rate in a C26a murine colon carcinoma. The sixteen IR-FLASH images of a C26a murine colon carcinoma (*left*). Plot of signal amplitudes from a single voxel within the tumor (*right*). The *dashed line* indicates the monoexponential fit ($R^2 = 0.9996$)

central slice through a C26a murine colon carcinoma. The acquisition time for the whole set of images was ca. 5 s. The combination of RF and gradient spoiling implemented in the IR-FLASH measurements provided images virtually free from artifacts. The signal intensity of the last image (image 16) was typically less than the signal intensity of the first image, due to small saturating effect originating from the read-out pulses. At the inversion time of approximately 1,000 ms, the longitudinal magnetization goes through the null point. The signal intensity changes from a single voxel within the tumor, as well as the fit of the signal recovery to a monoexponential function are illustrated in Fig. 1 (right). The R^2 value of 0.9996 indicates the excellent agreement between data points and fit.

To estimate the precision of the measured R_1 values of each tumor, four repeated measurements were performed prior to and following USPIO administration (Fig. 2). The column graph shows the values of R_1 obtained from the four repeated measurements prior to and following administration of USPIO, in a C26a and a C38 tumor. The horizontal line indicates the mean of the four measurements, while each point represents the value of one measurement. Prior to USPIO administration, $R_1 = 0.5467 \pm 0.0024\ s^{-1}$ in the C26a and $R_1 = 0.5791 \pm 0.0029\ s^{-1}$ in the C38. Following USPIO administration, $R_1 = 0.5692 \pm 0.0013\ s^{-1}$ in the C26a and $R_1 = 0.6596 \pm 0.0030\ s^{-1}$ in the C38. As a result, in both tumors, the USPIO-induced change ΔR_1 was greater than the SD value. The repeated measurements were performed in ten tumors. The results of the data analysis for all tumors are given in Table 1. The SD pre- and post-USPIO administration was typically ca. 1–3 $10^{-3}\ s^{-1}$. A small increase in SD in the post-USPIO measurements was observed. On the other hand, changes in R_1 induced by USPIO (third row in Table 1) were well above SD values in all cases.

In Fig. 3, a column graph of the changes in the R_1 relaxation rate following USPIO administration in all tumors showed a clear difference between C38 and C26a tumors. The R_1 increase in the C38 tumors ($\Delta R_1 = 0.072 \pm 0.0081\ s^{-1}$) was significantly larger than in the C26a tumors ($\Delta R_1 = 0.032 \pm 0.0018\ s^{-1}$,

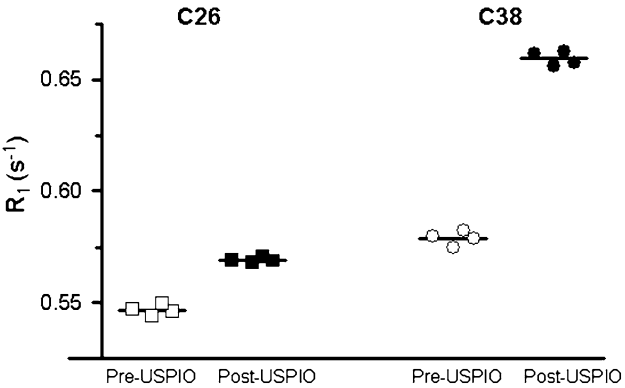

Fig. 2 Column graph of the changes in the R_1 relaxation rate following USPIO administration in a C26a and a C38 colon carcinoma. *Symbols* indicate the values of R_1 from four repeated measurements performed prior to and following USPIO administration. Prior to USPIO administration, in the example shown here, $R_1 = 0.5467 \pm 0.0024\ s^{-1}$ in the C26a and $R_1 = 0.5791 \pm 0.0029\ s^{-1}$ in the C38. Following USPIO administration, $R_1 = 0.5692 \pm 0.0013\ s^{-1}$ in the C26a and $R_1 = 0.6596 \pm 0.0030\ s^{-1}$ in the C38. In both tumors, the post-USPIO R_1 is significantly higher than pre-USPIO R_1

Table 1 SD of R_1 calculated from four repeated measurements, performed in ten tumors and the change in R_1 induced by the USPIO

	#1 (C38)	#2 (C38)	#3 (C38)	#4 (C38)	#5 (C38)	#6 (C26a)	#7 (C26a)	#8 (C26a)	#9 (C26a)	#10 (C26a)
$SD_{Pre\text{-}USPIO}$ ($[10^3\ s]^{-1}$)	1.2	2.9	0.6	2.5	1.1	1.5	2.4	1.0	0.9	1.3
$SD_{Post\text{-}USPIO}$ ($[10^3\ s]^{-1}$)	1.9	3.1	1.7	2.7	1.2	3.4	1.3	1.8	1.2	1.1
ΔR_1 ($[10^3\ s]^{-1}$)	84.1	99.8	45.1	72.2	59.5	33.7	23.1	27.9	30.4	26.3

The SD value provides an estimate of the precision of the in vivo measured values of R_1 in tumors, with the experimental setup employed in the current study. In the last row, the change in R_1 induced by the USPIO. In all cases, the SD value is well below the change in R_1 induced by the contrast agent

$P < 0.001$). Among the C26a tumors, changes in R_1 were very similar, while the C38 tumors displayed a broader range of changes in R_1. It should be noted that the smallest ΔR_1 observed in the C38 group was greater than the largest ΔR_1 of the C26a group.

The immunohistochemically determined RVA of the C38 tumors was larger than the RVA of the C26a tumors (0.059 ± 0.015 vs. 0.020 ± 0.011; $P = 0.0013$). This is illustrated in Fig. 4, which shows an RVA map, as well as the vascular structure, of a typical C38 and C26a tumor. The photomicrograph clearly shows the substantial difference in vascular volume and morphology between the C26a and C38 tumors.

Figure 5 shows the R_1 relaxation rate before USPIO administration and changes in the R_1 relaxation rate after USPIO and hydralazine administration. The increase in R_1 after USPIO administration was then followed by a decrease in R_1, after hydralazine administration.

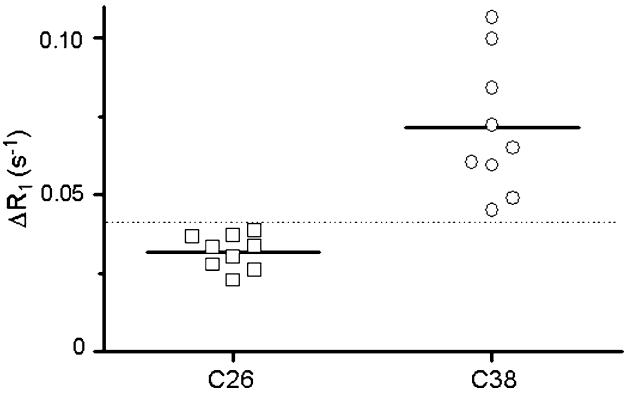

Fig. 3 Column graph of the changes in water proton R_1 relaxation rate (ΔR_1) following USPIO administration in the C26a and C38 colon carcinoma. The R_1 increase in the C38 ($\Delta R_1 = 0.072 \pm 0.0081\ s^{-1}$) was significantly larger than in the C26a colon carcinoma ($\Delta R_1 = 0.032 \pm 0.0018\ s^{-1}$, $P < 0.001$). The ΔR_1 in all C38 colon carcinoma was larger than $0.045\ s^{-1}$ (*dotted line*), while the ΔR_1 in all C26a colon carcinoma was smaller than this value

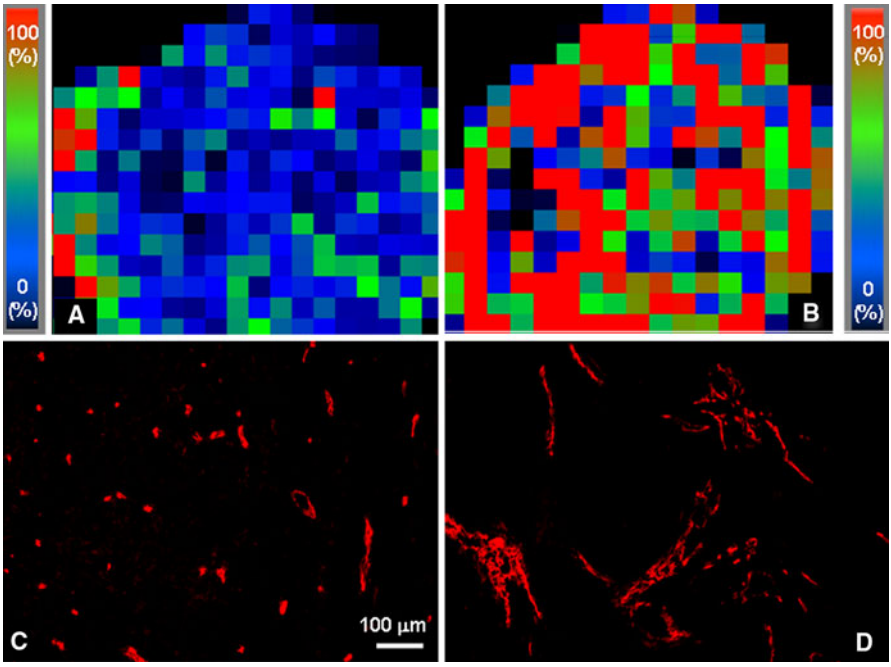

Fig. 4 RVA maps of the C26a (**a**) and C38 (**b**) tumor section. Each pixel represents a 0.23 × 0.23 mm ROI. Maps are scaled to 100% which corresponds to an RVA value of 21%. **c** and **d** Detailed photomicrographs of the tumors in **a** and **b**, showing the typical vascular structure of the C26a (**c**) and the C38 (**d**) colon carcinoma

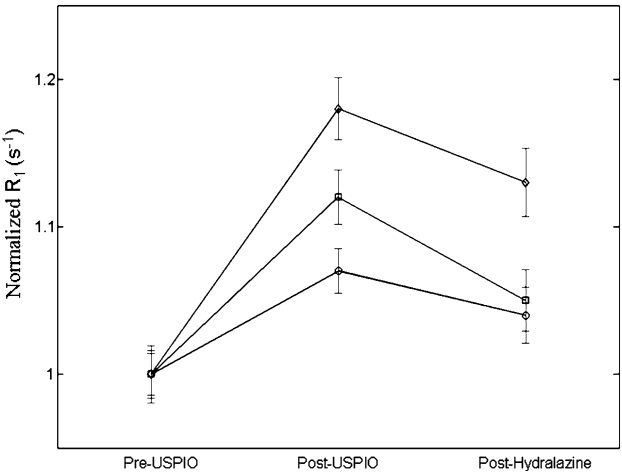

Fig. 5 Graph of normalized R_1 prior to USPIO administration (first time point), following USPIO administration (second time point) and 5 min after hydralazine administration (third time point) in three C38 colon carcinomas. Following hydralazine administration, R_1 decreased in all tumors, indicating a vasoconstriction effect

4 Discussion

In the current study, we propose a method which uses fast R_1 measurements on tumors prior to and following USPIO administration in order to monitor the tumor hemodynamics. While USPIO-induced changes in the transverse relaxation rates R_2 and R_2* within tumors have been experimentally investigated in a number of studies, less attention has been paid to quantitative measurements of R_1 changes [28]. Here, we first performed detailed measurements of R_1, to assess the precision of our experimental setup, in order to evaluate the significance of the R_1 changes. The high signal-to-noise ratio, achieved by (i) the use of a small surface coil, (ii) the positioning of the imaged slice in the plane of the coil itself and (iii) the high field strength, results in a reliable and precise measure of R_1. As a consequence, R_1 changes following USPIO are significantly larger than the experimental error associated with the R_1 measurement.

The USPIO-induced increase in R_1 may be attributed to the exchange of water protons between the intra- and extravascular space [19]. Following administration of USPIO, R_1 of the intravascular water protons in blood significantly increases (i.e., T_1 decreases from a value of ca. 2 s to a value below 200 ms [28]), whereas the extravascular water protons affected by the contrast agent are only those which are in exchange with the intravascular space. As a result, following USPIO administration, the value of $|R_{1i} - R_{1e}|$ increases to a value of ca. 5 Hz, which is greater than the suggested values of τ ($\sim$1 Hz [20–23]). Thus, USPIO administration drives the system towards slow exchange. In the limit of slow exchange, two decaying components are expected. However, since only about 5% of the water signal can be attributed to intravascular water protons and since the T_1 relaxation time of the intravascular component is very short, MRI using the inversion–recovery imaging

sequences cannot resolve the two decaying components, that is, it cannot detect the fast-decaying component. The measured T_1 is therefore representative of the extravascular component. In the case of slow exchange, as pointed out in Sect. 2, ΔR_1 is proportional to the blood volume and to the PS product. Therefore, differences in ΔR_1 between various tumor lines may be due to differences in blood volume, PS product or both. In our study, there was a statistically significant difference ($P < 0.001$) between ΔR_1 in the C26a and C38 colon carcinoma, with ΔR_1 being larger in the C38 than in the C26a colon carcinoma. This result indicates a difference in tumor vascular morphology between the two tumor lines, which is attributed either to differences in the PS product or in blood volume. The results from the immunohistochemistry, which was performed in the current study on the same tumor lines, indicate that there was a difference in RVA between the two tumor lines, with the C38 colon carcinoma exhibiting a higher RVA.

More relevant and of immediate interpretation are the R_1 changes for investigating hemodynamic effects in tumors. In fact, in case of vasoconstriction or vasodilation within the same tumor, ΔR_1 can be strictly related to vasoconstriction or vasodilation effects. In other words, if—as a response to a blood hemodynamic modifier—vasoconstriction (or vasodilation) occurs within the tumor, there will be a decrease (or increase) of both surface area and blood volume. Therefore, any vasoconstriction (or vasodilation) is reflected in a decrease (or increase) of R_1. The decrease in R_1 after hydralazine administration, which is a well-known central vasodilator, suggested a hydralazine-induced vasoconstriction in tumors. This is in line with the observation of vasoconstriction by the steal effect mechanism [29] due to hydralazine reported in other studies of subcutaneous tumors utilizing fluorescent staining [30] and contrast-enhanced MRI [31]. The 'paradoxical' vasoconstrictor effect (the 'steal effect') in tumor vasculature, as a result of administration of vasodilator agents, such as hydralazine for instance [29–31], can be explained in the following way: the systemic vasodilation of all 'healthy' blood vessels in the body takes away blood ("steal" the blood) from the tumor vasculature. In fact, since the tumor vasculature itself does not respond directly to the vasoactive agent, as it has a minimal capability of blood flow autoregulation [13], a reduction in tumor blood flow/volume is observed. Tumors have developed a number of ways to ensure a proper blood supply, such as incorporation of pre-existent vessels (also referred to as vessel co-option), vessel modulation (e.g., dilatation and intussusception) and angiogenesis [1, 8]. The ability to monitor tumor blood volume with a high temporal resolution in vivo will provide essential insight into tumor physiology and is a prerequisite to evaluate tumor response to therapy. It will further improve our knowledge of a tumor vasculature response to vasoactive agents (such as in serial measurements of CO_2/O_2 breathing experiments, for instance), tumor capability for blood flow autoregulation, and transient hemodynamic effects in tumors.

The most significant advantage of quantitative R_1 over quantitative R_2^*/R_2 measurements is the temporal resolution: a few seconds for R_1 measurements versus minutes in R_2 measurements. It should be noted that a temporal resolution of seconds could be also achieved with T_2^*/T_2-weighted imaging; on the other hand, measurement of relative changes in the signal intensity makes interindividual

comparison less reliable. With respect to fast quantitative T_2*/T_2 measurements, based on a steady-state free precession type of acquisition [32], for instance, they suffer from B_1 inhomogeneties and artifacts due to off-resonance (B_0 inhomogeneities), in particular, at high fields. Quantitative R_1 measurements could be an interesting alternative to T_2*/T_2-weighted images and quantitative R_2*/R_2 measurements in assessing changes in blood hemodynamics and thus can give novel insight into the effects of blood hemodynamic modifiers on tumor vasculature, non-invasively and with a high temporal resolution.

Acknowledgments We thank A. Veltien and B. Lemmers for technical assistance with the MRI measurements and animal handling. We also thank J. Lok, from the Department of Radiation Oncology for providing us with the photomicrographs of tumor vasculature. This work is supported by Dutch Cancer Society, grant KUN 2000-2307 and NWO-ZONWM investment grant 902-37-088.

References

1. J. Folkman, Semin. Cancer Biol. **3**(2), 65–71 (1992)
2. R.K. Jain, Cancer Res. **48**(10), 2641–2658 (1988)
3. J.H. Kaanders, J. Bussink, A.J. van der Kogel, Lancet Oncol. **3**(12), 728–737 (2002)
4. D.K. Kelleher, P.W. Vaupel, Radiother. Oncol. **32**(1), 47–53 (1994)
5. M.C. Hulshof, C.J. Rehmann, J. Booij, E.A. van Royen, D.A. Bosch, D. Gonzalez Gonzalez, Radiother. Oncol. **48**(2), 135–142 (1998)
6. C. Bremer, M. Mustafa, A. Bogdanov Jr., V. Ntziachristos, A. Petrovsky, R. Weissleder, Radiology **226**(1), 214–220 (2003)
7. J. Dennie, J.B. Mandeville, J.L. Boxerman, S.D. Packard, B.R. Rosen, R.M. Weisskoff, Magn. Reson. Med. **40**(6), 793–799 (1998)
8. G. Gambarota, W. Leenders, C. Maass, P. Wesseling, B. van der Kogel, O. van Tellingen, A. Heerschap, Br. J. Cancer **98**(11), 1784–1789 (2008)
9. G. Gambarota, H.W. van Laarhoven, M. Philippens, J. Lok, A. van der Kogel, C.J. Punt, A. Heerschap, Magn. Reson. Imaging **24**(3), 279–286 (2006)
10. G. Le Duc, M. Peoc'h, C. Remy, O. Charpy, R.N. Muller, J.F. Le Bas, M. Decorps, Magn. Reson. Med. **42**(4), 754–761 (1999)
11. S.P. Robinson, P.F. Rijken, F.A. Howe, P.M. McSheehy, B.P. van der Sanden, A. Heerschap, M. Stubbs, A.J. van der Kogel, J.R. Griffiths, J. Magn. Reson. Imaging **17**(4), 445–454 (2003)
12. I. Tropres, S. Grimault, A. Vaeth, E. Grillon, C. Julien, J.F. Payen, L. Lamalle, M. Decorps, Magn. Reson. Med. **45**(3), 397–408 (2001)
13. R.L. Jirtle, Int. J. Hyperthermia **4**(4), 355–371 (1988)
14. R. Deichmann, A. Haase, J. Magn. Reson. **96**(1), 608–612 (1992)
15. A. Haase, D. Matthaei, R. Bartkowski, E. Duhmke, D. Leibfritz, J. Comput. Assist. Tomogr. **13**(6), 1036–1040 (1989)
16. Y. Zur, M.L. Wood, L.J. Neuringer, Magn. Reson. Med. **21**(2), 251–263 (1991)
17. S. Nekolla, T. Gneiting, J. Syha, R. Deichmann, A. Haase, J. Comput. Assist. Tomogr. **16**(2), 327–332 (1992)
18. J.M. Bland, D.G. Altman, BMJ **312**(7047), 1654 (1996)
19. K.M. Donahue, R.M. Weisskoff, D. Burstein, J. Magn. Reson. Imaging **7**(1), 102–110 (1997)
20. C.S. Landis, X. Li, F.W. Telang, P.E. Molina, I. Palyka, G. Vetek, C.S. Springer Jr, Magn. Reson. Med. **42**(3), 467–478 (1999)
21. H.B. Larsson, S. Rosenbaum, T. Fritz-Hansen, Magn. Reson. Med. **46**(2), 272–281 (2001)

22. O.B. Paulson, M.M. Hertz, T.G. Bolwig, N.A. Lassen, Acta Neurol. Scand. Suppl. **64**, 492–493 (1977)
23. C.M. Wacker, F. Wiesmann, M. Bock, P. Jakob, J.J. Sandstede, A. Lehning, G. Ertl, L.R. Schad, A. Haase, W.R. Bauer, Magn. Reson. Med. **47**(5), 1013–1016 (2002)
24. C. Schwarzbauer, S.P. Morrissey, R. Deichmann, C. Hillenbrand, J. Syha, H. Adolf, U. Noth, A. Haase, Magn. Reson. Med. **37**(5), 769–777 (1997)
25. J.R. Westphal, R.G. van't Hullenaar, J.A. van der Laak, I.M. Cornelissen, L.J. Schalkwijk, G.N. van Muijen, P. Wesseling, P.C. de Wilde, D.J. Ruiter, R.M. de Waal, Br. J. Cancer **76**(5), 561–570 (1997)
26. J. Bussink, J.H. Kaanders, P.F. Rijken, C.A. Martindale, A.J. van der Kogel, Br. J. Cancer **77**(1), 57–64 (1998)
27. P.F. Rijken, H.J. Bernsen, A.J. van der Kogel, Microvasc. Res. **50**(2), 141–153 (1995)
28. E.L. Barbier, K.S. St Lawrence, E. Grillon, A.P. Koretsky, M. Decorps, Magn. Reson. Med. **47**(6), 1100–1109 (2002)
29. W.D. Voorhees 3rd, C.F. Babbs, Eur. J. Cancer Clin. Oncol. **18**(10), 1027–1033 (1982)
30. M.J. Trotter, B.D. Acker, D.J. Chaplin, Int. J. Radiat. Oncol. Biol. Phys. **17**(4), 785–789 (1989)
31. C.A. Belfi, L.L. Ting, S.J. Hassenbusch, M. Tefft, F.Q. Ngo, Int. J. Radiat. Oncol. Biol. Phys. **22**(3), 477–482 (1992)
32. S.C. Deoni, T.M. Peters, B.K. Rutt, Magn. Reson. Med. **53**(1), 237–241 (2005)